THE JOURNAL OF BIOLOGICAL CHEMISTRY VOL. 289, NO. 24, pp. 16867–16882, June 13, 2014

Kinetics, Structure, and Mechanism of 8-Oxo-7,8-dihydro-2′-deoxyguanosine Bypass by Human DNA Polymerase η*◆

Received for publication, January 22, 2014, and in revised form, April 14, 2014 Published, JBC Papers in Press, April 23, 2014, DOI 10.1074/jbc.M114.551820

Amritraj Patra‡, Leslie D. Nagy‡, Qianqian Zhang‡, Yan Su‡, Livia Müller§, F. Peter Guengerich‡, and Martin Egli‡1

From the ‡Department of Biochemistry and Center in Molecular Toxicology, Vanderbilt University School of Medicine, Nashville, Tennessee 37232 and the §Laboratory of Food and Nutrition Toxicology, Eidgenössische Technische Hochschule-Zentrum, CH-8092 Zürich, Switzerland

Background: 8-OxoG is a major oxidative lesion in DNA and is associated with cancer.
Results: Kinetic and mass spectrometric studies demonstrate that human polymerase η bypasses 8-oxoG in a largely error-free manner.
Conclusion: Arginine 61 from the finger domain plays a key role in error-free bypass at the insertion stage.
Significance: In addition to photo-adducts and cisplatinated DNA, polymerase η might also be involved in accurate bypass of 8-oxoG *in vivo*.

DNA damage incurred by a multitude of endogenous and exogenous factors constitutes an inevitable challenge for the replication machinery. Cells rely on various mechanisms to either remove lesions or bypass them in a more or less error-prone fashion. The latter pathway involves the Y-family polymerases that catalyze trans-lesion synthesis across sites of damaged DNA. 7,8-Dihydro-8-oxo-2′-deoxyguanosine (8-oxoG) is a major lesion that is a consequence of oxidative stress and is associated with cancer, aging, hepatitis, and infertility. We have used steady-state and transient-state kinetics in conjunction with mass spectrometry to analyze *in vitro* bypass of 8-oxoG by human DNA polymerase η (hpol η). Unlike the high fidelity polymerases that show preferential insertion of A opposite 8-oxoG, hpol η is capable of bypassing 8-oxoG in a mostly error-free fashion, thus preventing GC→AT transversion mutations. Crystal structures of ternary hpol η-DNA complexes and incoming dCTP, dATP, or dGTP opposite 8-oxoG reveal that an arginine from the finger domain assumes a key role in avoiding formation of the nascent 8-oxoG:A pair. That hpol η discriminates against dATP exclusively at the insertion stage is confirmed by structures of ternary complexes that allow visualization of the extension step. These structures with G:dCTP following either 8-oxoG:C or 8-oxoG:A pairs exhibit virtually identical active site conformations. Our combined data provide a detailed understanding of hpol η bypass of the most common oxidative DNA lesion.

7,8-Dihydro-8-oxo-2′-deoxyguanosine (8-oxoG)[2] is one of the most common DNA lesions resulting from oxidative stress during normal aerobic cellular metabolism (1–3). It is found in both lower organisms and eukaryotes and is relevant because of its association with cancer (4, 5), aging (6), hepatitis (7), and infertility (8). Compared with G and the canonical G:C pairing mode, the presence of oxygen at the C8-position in 8-oxoG alters the nucleoside conformational equilibrium between the *anti* and *syn* modes in favor of the latter, thus enabling pairing with A. This effect constitutes the basis for the mutagenicity of 8-oxoG due to the resulting G:C to T:A transversion mutations (9, 10). Among the cellular responses dealing with oxidative damage such as 8-oxoG, mismatch repair (MMR) assumes an important role (11). In yeast, the Ogg1 glycosylase is known to remove the 8-oxoG lesion opposite C in double-stranded DNA (12, 13). Conversely, when A is replicated opposite 8-oxoG in yeast, it is recognized and excised by MutSα (14).

Lesions that evade recognition and repair prior to replication can elicit trans-lesion synthesis (TLS) (15–18). TLS involves the Y-family of DNA polymerases (pols) (19, 20), with four members identified in humans, pol η, pol ι, pol κ, and Rev 1, which exhibit various propensities and fidelities in the bypass of individual lesions (20–23). Detailed structural and functional investigations have shed light on the characteristics of these TLS pols and revealed clear differences among them in terms of their mechanisms of adduct bypass (21, 24). Although Y-family pols share the right-handed arrangement of palm, thumb, and finger subdomains (25) with high fidelity pols (*i.e.* A-family), they also feature a distinct "little finger" (LF) or pol-associated domain that is crucial for lesion bypass (24, 26–29). TLS pols generally exhibit lower processivity, catalytic efficiency, and

* This work was supported, in whole or in part, by National Institutes of Health Grants ES010375 (to F. P. G. and M. E.), P01 CA160032 (to M. E.), and P30 ES000267 (to F. P. G. and M. E.).
◆ This article was selected as a Paper of the Week.
The atomic coordinates and structure factors (codes 4O3N, 4O3O, 4O3P, 4O3Q, 4O3R, and 4O3S) have been deposited in the Protein Data Bank (http://wwpdb.org/).
[1] To whom correspondence should be addressed: Dept. of Biochemistry and Center in Molecular Toxicology, Vanderbilt University School of Medicine, 868A Robinson Research Bldg., Nashville, TN 37232-0146. Tel.: 615-343-8070; Fax: 615-322-7122; E-mail: martin.egli@vanderbilt.edu.

[2] The abbreviations used are: 8-oxoG, 7,8-dihydro-8-oxo-2′-deoxyguanosine; pol, (DNA) polymerase; hpol, human polymerase; Dpo4, *S. solfataricus* DNA polymerase IV; TLS, trans-lesion synthesis; MMR, mismatch repair; LF, little finger; CID, collision-induced dissociation; dNMPNPP, 2′-deoxynucleoside-5′-[(α,β)-imido]triphosphate; dTMPNPP, 2′-deoxythymidine-5′-[(α,β)-imido]triphosphate; dCMPNPP, 2′-deoxycytidine-5′-[(α,β)-imido] triphosphate; dAMPNPP, 2′-deoxyadenosine-5′-[(α,β)-imido]triphosphate; dGMPNPP, 2′-deoxyguanosine-5′-[(α,β)-imido]triphosphate.

copying fidelity on undamaged DNA than high fidelity pols. However, we observed that the pol κ homolog Dpo4 from *Sulfolobus solfataricus* bypasses 8-oxoG with high fidelity (19:1 ratio of dCTP:dATP incorporation opposite 8-oxoG) and efficiency (pre-steady-state kinetics revealed faster rates of dCTP incorporation opposite 8-oxoG than G) (30) that could be attributed to a significant extent to Arg-332 from the LF domain (31). By comparison, we established that human pol κ (hpol κ) bypasses 8-oxoG in an error-prone fashion, with dATP rather than dCTP preferentially incorporated opposite the lesion (32). Its proclivity to insert A opposite 8-oxoG resembles the action of replicative polymerases (33, 34).

Among the eukaryotic TLS pols, pol η is considered to play an important role in 8-oxoG bypass, although initial assays using human large-cell carcinoma cell line H1299 and xeroderma pigmentosum variant (defective in pol η) cells showed that the nucleotide inserted opposite 8-oxoG was the correct C at frequencies of 81 and 77%, respectively (35). However, mutation frequencies were increased in mammalian GM637 and in xeroderma pigmentosum variant cells in the presence of siRNA targeting pol η (36). Interestingly, in the same system knockdown of MMR glycosylase OGG_1 also triggered an increase in mutagenesis, providing support for the hypothesis that both the MMR and TLS systems combat mutagenic damage due to 8-oxoG. Overlaps between MMR and TLS were confirmed by a recent *in vivo* study in yeast. The A residues opposite 8-oxoG were removed by MMR, subsequently triggering re-replication and, in the absence of MMR, by pol η TLS, with an accuracy of insertion of dCTP opposite 8-oxoG of 94% (37).

Other investigators using yeast-based assays and/or the enzyme from yeast observed accurate and efficient bypass of 8-oxoG by pol η (38), whereby C, A, or G was incorporated opposite 8-oxoG with a relative efficiency of 100:56:14 (39). Moreover, pol η binds dCTP opposite both G and 8-oxoG with similar affinities and inserts the correct nucleotide opposite both G and 8-oxoG with similar rates (40). Structural data for the complexes between yeast pol η with 8-oxoG:C (bound at the insertion and extension stages) were in line with the relatively accurate bypass of 8-oxoG by this enzyme but allowed no comparison with insertion of dATP opposite 8-oxoG or extension from 8-oxoG:A (41). An investigation entailing six human B-, X-, and Y-family pols established that (relative to dATP) correct incorporation of dCTP opposite 8-oxoG in the presence of the proliferating cell nuclear antigen and replication protein A auxiliary proteins is 1,200- and 68-fold more efficient for pol λ and pol η, respectively (42). An important role of pol λ in combination with pol δ for bypass of 8-oxoG was also established *in vitro* using mouse embryonic fibroblasts and HeLa cells (43).

The somewhat inconsistent observations regarding the accuracy of 8-oxoG bypass catalyzed by pol η in cells are mirrored by the results from *in vitro* primer extension experiments probing its ability to correctly insert dCTP instead of dATP. Yung *et al.* (44) tested the bypass of 8-oxoG by human pol η (hpol η) *in vitro* in four different sequence contexts and found that the identity of the nucleotide 5′-adjacent to 8-oxoG had a significant effect on the incorporation efficiency and accuracy. Thus, for the sequences 5′-oligo-CG*X*, -CC*X*, -CA*X*, and -CT*X* (*X* = 8-oxoG), the dC:dA ratio varied between 1.1 and 2.9 (lowest for CA*X* and highest for CC*X*). However, the efficiency was lowest for the CC*X* and highest for the CA*X* oligonucleotide. Conversely, the dC:dG ratio was lowest for the CA*X* (2.0) and highest for the CG*X* oligonucleotide (7.7). Using a 30-mer oligonucleotide with a single 8-oxoG for *in vitro* bypass, Zhang *et al.* (45) observed relatively error-prone insertion opposite 8-oxoG by hpol η (dC:dA ≈1:1 based on V_{max}/K_m) as well as similar efficiencies for extension from either 8-oxoG:C or 8-oxoG:A (5:3). Using oligonucleotides corresponding to a region of the human *c-Ha-ras* gene and containing either one or two 8-oxoG residues, Jaloszynski *et al.* (46) found that the ratios between the efficiencies (k_{cat}/K_m) of dC and dA incorporation opposite the adduct varied between 8.5 and 2.4 (C > A). The lower ratio is similar to the results obtained by McCulloch *et al.* (47), who reported that the pol η enzymes from mouse and human show error rates for *in vitro* bypass of 8-oxoG that approach 50%, in line with the data by others that support similar efficiencies for insertion of either dC or dA opposite 8-oxoG as well as for the extension of the resulting pairs by the human enzyme (42, 45). Clearly, these results are inconsistent with the error-free bypass of 8-oxoG by pol η. Thus, the enzyme appears (based on this literature) to have inherently less fidelity than Dpo4, which synthesizes past the lesion with high accuracy and efficiency.

pol η displays an unmatched ability to replicate past UV-induced cyclic pyrimidine dimers (48), and a deficiency in the polymerase is the basis for a variant form of the human syndrome xeroderma pigmentosum, characterized by a highly elevated occurrence of skin malignancies (49, 50). pol η also facilitates TLS past cancer drug adducts such as cisplatin (51) and thus lowers the cellular sensitivity to treatment. Structural studies on hpol η have focused on complexes of the catalytic core with DNA template-primer constructs containing *cis-syn* cyclobutane thymine dimers and have disclosed how the polymerase accommodates two nucleotides at the active site (52). Elegant work by Yang and co-workers (53) has provided insight into the step-by-step mechanism of pol η bypass and phosphodiester bond formation. Crystal structures of the enzymes from yeast (54) and human (55), in complex with cisplatin-modified DNA, have also provided a better understanding of the correct insertion of dCTP opposite the distorted cross-linked G dimer and the efficient extension after the lesion. No structures of hpol η in complex with DNA containing the 8-oxoG adduct have been reported to date.

To evaluate the efficiency and accuracy of *in vitro* bypass of 8-oxoG by hpol η, we carried out a comprehensive analysis of the bypass activity of the catalytic core of the enzyme, including steady-state and pre-steady-state kinetics of primer extension opposite and beyond 8-oxoG and LC-MS/MS assays of full-length extension products. To gain a better understanding of the mechanism of 8-oxoG bypass by hpol η, we determined crystal structures of the native hpol η complex (G:dCTP; reference structure), three insertion-stage complexes with 8-oxoG paired to dCTP, dATP, or dGTP, and two complexes capturing the extension steps following 8-oxoG:C or 8-oxoG:A. Our analysis demonstrates that hpol η inserts almost exclusively dCTP opposite template 8-oxoG, with Arg-61 from the finger domain playing a crucial role in the discrimination against dATP, and

that the polymerase achieves error-free bypass of the 8-oxoG lesion at the insertion stage.

EXPERIMENTAL PROCEDURES

Materials—All unlabeled dNTPs were obtained from Amersham Biosciences, and [γ-^{32}P]ATP was purchased from PerkinElmer Life Sciences. All nonhydrolyzable dNMPNPPs were obtained from Jena Bioscience (Jena, Germany). All oligonucleotides used in this work were synthesized by Midland Certified Reagent Co. (Midland, TX), TriLink Biotechnologies (San Diego), or Integrated DNA Technologies (Coralville, IA), and in some cases they were purified using HPLC by the manufacturer, with analysis by matrix-assisted laser desorption time-of-flight MS.

hpol η Catalytic Core Protein Expression and Purification—The hpol η plasmid (pET28a) comprising residues 1–432 was a generous gift from Dr. Wei Yang, NIDDK, National Institutes of Health. The polymerase was expressed in *Escherichia coli* and purified as described previously (52). The protein solution was concentrated to 5 mg/ml.

Steady-state Kinetics—Steady-state incubation typically included 2.5–10 nM hpol η, 5 μM template-primer oligonucleotide mixture as substrate (the primer was 5′-6-carboxyfluorescein-labeled, and template-primer duplexes (1:1 molar ratio) were pre-annealed by heating and slow cooling), 40 mM Tris-HCl buffer (pH 7.5), 100 mM KCl, 5 mM $MgCl_2$, 10 mM DTT, 5% glycerol (v/v), 100 μg/ml bovine serum albumin (BSA), and varying concentrations of a single dNTP (added last to start the reaction). The incubation temperature was 37 °C, and reactions were typically run for 5 min (or less to keep product formation <20% of the oligonucleotide substrate concentration). Reactions were quenched by the addition of a quench reagent containing formamide, EDTA, bromphenol blue, and xylene cyanol (56), and aliquots were applied to an 18% (w/v) acrylamide, 7.5 M urea gel and separated by electrophoresis. Fluorescence in the substrate and product primer bands was scanned using a Typhoon system (GE Healthcare) and quantified by ImageJ (National Institutes of Health), and the data were fit to hyperbolic plots (Michaelis-Menten equation) using the program GraphPad Prism (GraphPad, La Jolla, CA).

Pre-steady-state Kinetics—A KinTek RP-3 instrument was used, utilizing general procedures described previously (56). In a typical experiment, 50 nM hpol η was incubated with 500 nM oligonucleotide (5′-^{32}P-primer/unlabeled template) and rapidly mixed with 0.5 mM dNTP in the same buffer system used in the steady-state kinetic studies (see above), incubated for varying lengths of time (10 ms to 5 s), and quenched by the addition of 0.5 mM EDTA (from the quench line). Radioactivity in the substrate and product primer bands was quantified using a phosphorimager system (Bio-Rad), and the data were fit with the log-linear relationship $y = Ae^{kpt} + k_{ss}$, where k_p is the first-order rate for the first catalytic cycle; k_{ss} is the steady-state rate, and A is the extent of the product burst (GraphPad Prism).

LC-MS/MS Analysis of Full-length Extension Products—Six different template-primer complexes were used, based upon literature precedents for work with hpol η and 8-oxoG (*X*) as follows: 5′-TCGTAAGCGTC*U*T-3′ and 3′-AGCATTCGCAGTA*X*TACT-5′ (this work); 5′-CGGCCTCCGGA*U*C-3′ and 3′-GCCGGAGGCCTAG*X*ACGT-5′ (45); 5′-TTGCCCACACC*U*C-3′ and 3′-AACGGGTGTGGCG*X*CCGC-5′ (46); 5′-GCCATGGCCCA*U*T-3′ and 3′-CGGTACCGGGTTA*X*CCTT-5′ (47); 5′-TGCCGAATTCA*U*A-3′ and 3′-ACGGCTTAAGTGT*X*GCAG-5′ (42); and 5′-GCCCAGGGTTT*U*C-3′ and 3′-CGGGTCCCAAAAG*X*GTCA-5′ (35). In all cases, uracil (*U*) was included in the primer to facilitate cleavage of the product to a shorter form that could be analyzed (following cleavage with uracil DNA glycosylase and then hot piperidine) in an ion-trap mass spectrometer (57–59). hpol η (1.6 nmol) was reacted with each (5′-5/6-carboxyfluorescein-labeled) template-primer complex (2 nmol) and a mixture of 1 mM each of dATP, dCTP, dGTP, and dTTP at 37 °C for 4 h in 50 mM Tris-HCl buffer (pH 7.5). The reactions were terminated by spin column separations to extract dNTPs and Mg^{2+}. The extent of the reaction was checked by electrophoresis/fluorography prior to LC-MS analysis. The resulting product was treated with 25 units of uracil DNA glycosylase and 0.25 M piperidine following a previous protocol (57–59). To identify the products, the resulting reactions were analyzed by LC-MS/MS using an Acquity UPLC system (Waters) interfaced to a Thermo-Finnigan LTQ mass spectrometer (Thermo Scientific, San Jose, CA) equipped with a negative ion electrospray source. Chromatographic separation was achieved with the Acquity UPLC BEH octadecylsilane (C_{18}) column (1.0 × 100 mm, 1.7 μm). The LC conditions were as follows: mobile phase A, 10 mM $NH_4CH_3CO_2$ in 98% H_2O; mobile phase B, 10 mM $NH_4CH_3CO_2$ in 95% CH_3CN (v/v). The following gradient program (v/v) was used with a flow rate of 200 μl min^{-1}: the gradient started with 2% B (v/v), increased to 10% B (v/v) at 5 min, increased to 20% B (v/v) at 9 min, and held at 30% B (v/v) for 1 min. The column was re-equilibrated for 3 min with 5% B (v/v). The temperature of the column was maintained at 50 °C. MS conditions were as follows: source voltage, 4 kV; source current 100 μA; capillary voltage, −49 V; capillary temperature, 350 °C; tube lens voltage, −90 V. Product ion spectra were acquired over the range *m/z* 300–2,000, and the most abundant species (−2 charge) was used for collision-induced dissociation (CID) analysis. The most abundant species (−2 or −3 charged) were used for CID analysis; calculation of the CID fragmentation of the oligonucleotide sequence was done using a program linked to the Mass Spectrometry Group of Medicinal Chemistry at the University of Utah; the Mongo Oligo Mass Calculator (version 2.6) from the University of Utah was used to calculate the theoretical CID spectra of the candidate oligonucleotide sequences. The relative yields of various products were calculated based on the peak areas of extracted ion chromatograms from LC-MS analyses. The sum of the peak areas was used for multicharged species.

Crystallizations—Primer and template sequences used in the crystallization experiments are listed in Table 6. 8-OxoG-modified DNA templates were purchased from TriLink (San Diego), and unmodified 8-mer primers were obtained from Integrated DNA Technologies (Coralville, IA). Template and primer strands were mixed in a 1:1 molar ratio and were annealed in the presence of 10 mM sodium HEPES buffer (pH 8.0), 0.1 mM EDTA, and 50 mM NaCl by heating for 10 min at 85 °C followed

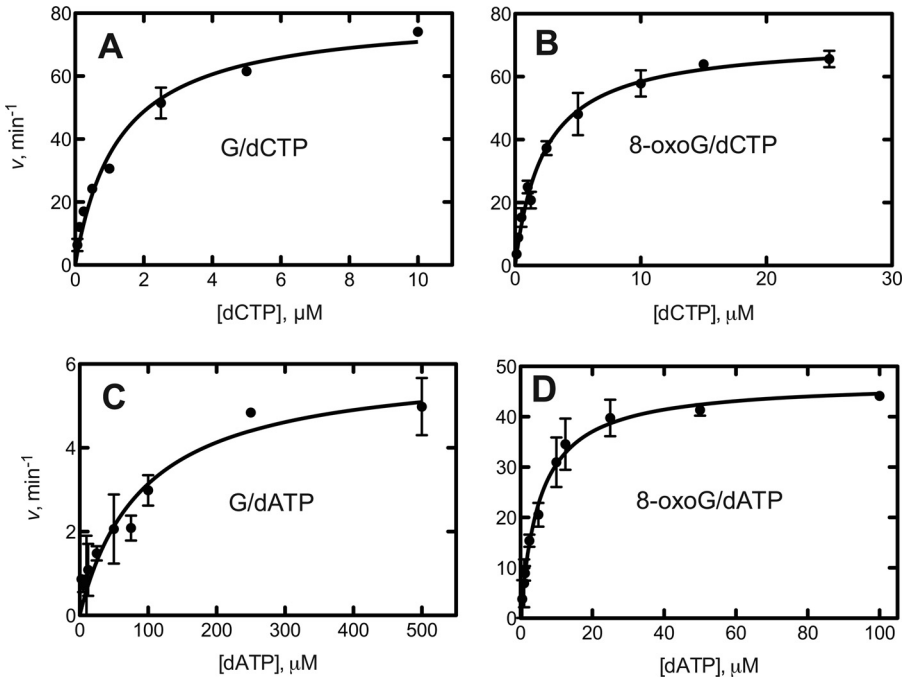

FIGURE 1. **Steady-state kinetic analysis of dNTP incorporation by hpol η.** The reaction contained a template with G or 8-oxoG at position *X* as follows: 5′-CGGTCGTAAGCGTCAT-3′ and 3′-GCCAGCATTCGCAGTA*X*TACT-5′. hpol η (2.5–10 nM) was used with an oligonucleotide concentration of 5 μM and varying concentrations of dATP or dCTP. Incubation proceeded for 5 min at 37 °C, and products formed were seperated by PAGE. All reactions were done in duplicate, and the indicated data points are shown as means ± standard deviation. *A*, dCTP incorporation opposite G; *B*, dCTP incorporation opposite 8-oxoG; *C*, dATP incorporation opposite G. *D*, dATP incorporation opposite 8-oxo G. See Table 1 for k_{cat} and K_m values (estimated using fit to a hyperbolic equations in Prism, GraphPad, San Diego).

by slow cooling to room temperature. For crystallization, the DNA duplex was mixed with the protein in a 1.2:1 molar ratio in the presence of excess 50 mM Tris-HCl buffer (pH 7.5) containing 450 mM KCl and 3 mM DTT. After adding 5 μl of 100 mM $MgCl_2$, the complex was concentrated to a final concentration of ~2–3 mg/ml by ultrafiltration. Nonhydrolyzable nucleotide triphosphates were added last to form ternary complexes. Crystallization experiments were performed by the hanging drop vapor diffusion technique at 18 °C using a sparse matrix screen (Hampton Research, Aliso Viejo, CA) (60). One μl of the complex solution was mixed with 1 μl of reservoir solution and equilibrated against 500-μl reservoir wells. Crystals appeared in droplets containing 0.1 M MES (pH 5.5) buffer containing 5 mM $MgCl_2$ and 15–17% (w/v) PEG 2000 MME within 1 day and grew to maximum size within a week.

X-ray Diffraction Data Collection, Structure Determination, and Refinement—Crystals were mounted in nylon loops, cryoprotected in reservoir solution containing 25% glycerol (v/v), and frozen in liquid nitrogen. Diffraction data were collected either on the 21-ID-D or the 21-ID-F beamline of the Life Sciences Collaborative Access Team at the Advanced Photon Source, Argonne National Laboratory (Argonne, IL). Data were integrated and scaled with the program HKL2000 (61). The structures were determined by the molecular replacement technique using the program MOLREP (62, 63) and the hpol η structure with Protein Data Bank code 4ECQ (protein alone) as the search model. Structure refinement and model building were carried out with PHENIX (64) and COOT (65), respectively. Illustrations were generated with the program UCSF Chimera (66).

TABLE 1

Steady-state kinetics of incorporation of dCTP, dATP, and dGTP opposite G and 8-oxoG by hpol η

Template base	dNTP	k_{cat}	K_m	k_{cat}/K_m	f^a
		s^{-1}	μM	$\mu M^{-1} s^{-1}$	
G	dCTP	1.33 ± 0.05	1.3 ± 0.2	1.0 ± 0.16	
G	dATP	0.10 ± 0.01	92 ± 23	0.0011 ± .0003	0.001
G	dGTP	0.15 ± 0.02	80 ± 34	0.0019 ± 0.0008	0.0019
8-OxoG	dCTP	1.20 ± 0.03	2.3 ± 0.2	0.52 ± 0.05	
8-OxoG	dATP	0.78 ± 0.03	5.4 ± 0.6	0.15 ± 0.02	0.28
8-OxoG	dGTP	0.43 ± 0.02	27 ± 5	0.016 ± 0.003	0.031

[a] $f = (k_{cat}/K_m)_{dNTP}/(k_{cat}/K_m)_{dCTP}$.

RESULTS

Kinetics of Incorporation of dCTP and dATP Opposite Template G and 8-OxoG by hpol η—For all kinetic and structural assays, we used the catalytic core construct of hpol η that includes amino acids 1–432 (52). In the steady-state kinetic analysis, hpol η preferably inserted dCTP opposite G with >99% fidelity, relative to dATP (Fig. 1 and Table 1). In the case of template 8-oxoG, dCTP was inserted 3.5-fold more efficiently than dATP. The catalytic efficiency of dCTP insertion opposite 8-oxoG was thus significantly higher than dATP insertion (k_{cat}/K_m 0.52 *versus* 0.15 $\mu M^{-1} s^{-1}$, Table 1). By comparison, the efficiency of insertion of dGTP opposite 8-oxoG was drastically lower but clearly elevated (~16-fold) relative to insertion of dGTP opposite template G (Table 1).

The enhanced ability of hpol η to incorporate dCTP opposite template 8-oxoG (relative to G) was also observed in pre-steady-state kinetic experiments (Fig. 2 and Table 2). Bursts were seen for incorporation of dCTP opposite G or 8-oxoG, but this was not the case for insertion of dATP opposite 8-oxoG

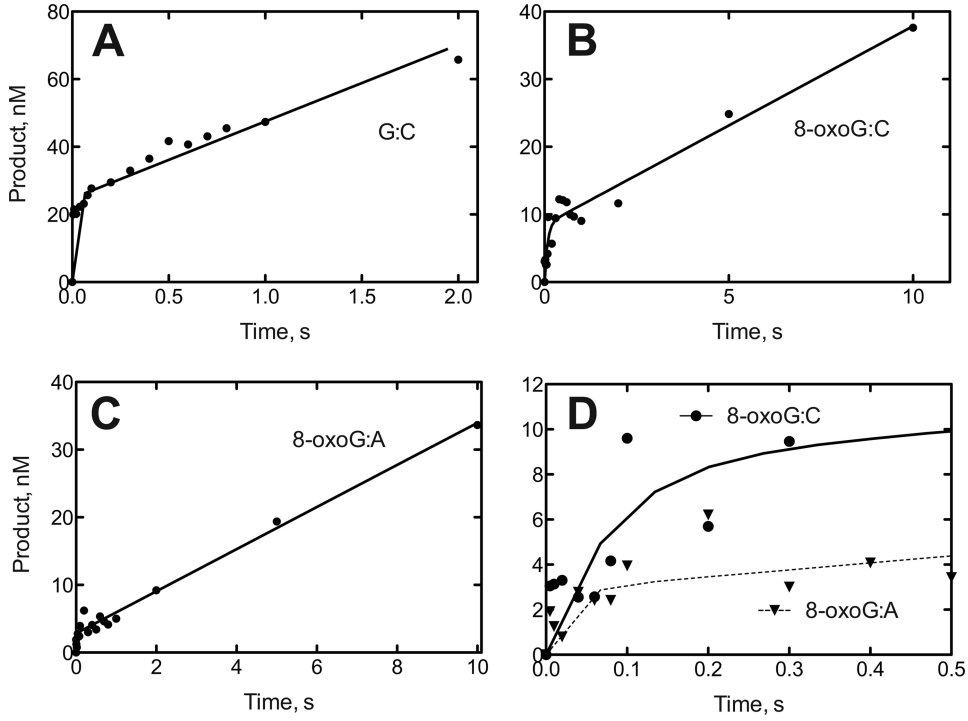

FIGURE 2. **Pre-steady-state kinetic analysis of dNTP incorporation by hpol η.** *A*, template G and incoming dCTP. *B*, template 8-oxoG and incoming dCTP. *C*, template 8-oxoG and incoming dATP. *D*, expansion of early phases of *B* (●–●) and *C* (▼–▼). The template-primer complexes of Fig. 1 were used (500 nM) with 50 nM hpol η, with the same buffer system (37 °C) and 0.5 mM dCTP or dATP, for the indicated times, and quenched by the addition of 500 mM EDTA. Products were analyzed by PAGE and phosphorimaging. Data points are shown as means of duplicate incubations and were fit to the equation $y = Ae^{kpt} + k_{ss}$, where k_p is the first-order rate for the first catalytic cycle; k_{ss} is the steady-state rate, and *A* is the extent of the product burst (GraphPad Prism).

TABLE 2
Burst kinetics of incorporation of dCTP and dATP opposite template G and 8-oxoG

Template base	dNTP	k_p	k_{ss}	Burst amplitude[a]
		s^{-1}	s^{-1}	nM
G	dCTP	>70[b]	0.45 ± 0.03	25 ± 1
8-OxoG	dCTP	12 ± 5	0.0045 ± 0.05	8.5 ± 0.8
8-OxoG	dATP[c]			

[a] The concentration of hpol η was 50 nM, based on A_{280} data.
[b] The estimate is made because the $t_{½}$ of the reaction was ≤10 ms, the effective dead time in the instrument under the operating conditions used here.
[c] The data did not fit well to a burst equation (Fig. 2*D*).

(the dATP analysis was not done with template G). The pre-steady-state rates of incorporation were faster for dCTP incorporation opposite G than 8-oxoG (>70 *versus* 12 s^{-1}). These rates are similar to that measured for full-length hpol η with a different sequence (30 s^{-1}) (67). In the case of incorporation opposite G, the burst amplitude was only ~50% of the concentration of hpol η (Fig. 2 and Table 2). With 8-oxoG in the template, the dCTP incorporation burst was ~17% the amount of hpol η (Fig. 2 and Table 2).

A higher efficiency of incorporation of dCTP opposite 8-oxoG (than G) was previously observed with *S. solfataricus* Dpo4 (30), but the opposite pattern was seen here, despite the tendency to insert dCTP in both cases. The substoichiometric bursts and the difference in burst amplitudes could be attributed to possible higher affinity of the G-containing oligonucleotide for hpol η (relative the 8-oxoG-containing oligonucleotide); an alternative explanation is that hpol η-oligonucleotide complexes have alternative nonproductive conformations and that these are favored with 8-oxoG. However, we do not have any further evidence to support this explanation at this point.

LC-MS/MS Analysis of Full-length Extension Products Produced by hpol η—Analysis of single insertions by a DNA polymerase is useful but may not reflect incorporation events at further sites, *i.e.* extension. We applied an LC-MS/MS approach developed in this laboratory to analyze the identity of individual extended primer sequences in more detail (57–59). In addition to the oligonucleotide that was utilized in the kinetic and crystallography experiments reported here, we included five sequences that had been assessed with hpol η and 8-oxoG in the literature and for which varying misincorporation results were reported by other authors (in various types of other assays) (Figs. 3 and 4 and Tables 3, 4, and summarized in Table 5) (35, 42, 45–47). The MS-based analysis revealed that A incorporation occurs at levels that range from <1 to 20% (Table 5). The highest level was seen with template 5′-A*X*G-3′ (only three nucleotides shown; *X* = 8-oxoG) (20% A), followed by 5′-G*X*T-3′ (17% A), 5′-C*X*G-3′ (10% A), 5′-C*X*A-3′ (3% A), 5′-G*X*G-3′ (<1% A), and 5′-T*X*A-3′ (<1% A; this work). In all cases hpol η continued to replicate the template strand in an error-free manner after inserting either C or A opposite 8-oxoG. Thus, extension of an A:8-oxoG pair is not associated with subsequent mismatch pairs or frameshifts.

X-ray Crystallography of Ternary hpol η-DNA-dNTP Insertion-step Complexes—To gain insight into the active site properties of hpol η underlying its mostly error-free bypass of 8-oxoG, we studied the crystal structures of three complexes between the polymerase and the dodecamer template 5′-d(CAT

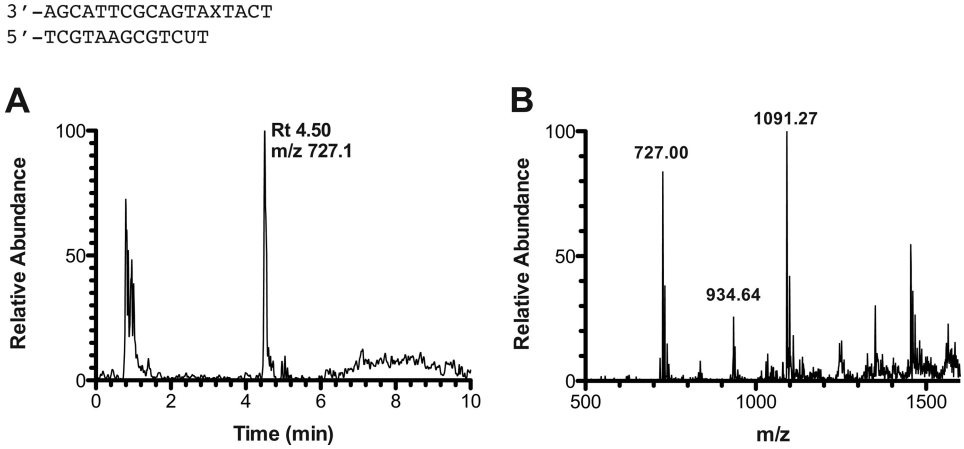

FIGURE 3. **LC-MS analysis of full-length extension products by hpol η in the presence of all four dNTPs.** *A*, sample reconstructed extracted ion chromatogram for *m/z* 727.1 (−3) for product with sequence 5′-TCATGAA-3′. *B*, mass spectrum of peak at retention time 4.42 min. See Table 3 for full list of products and respective *m/z* assignments.

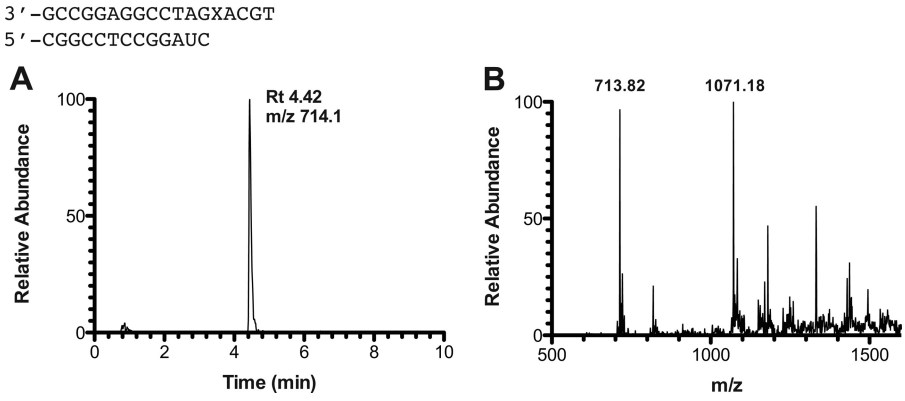

FIGURE 4. **LC-MS analysis of full-length extension products by human pol η in the presence of all four dNTPs.** *A*, sample reconstructed extracted ion chromatogram for *m/z* 714.1 (−3) for product with sequence 5′-CCTGCAA-3′. *B*, mass spectrum of peak at retention time 4.42 min. See Table 4 for full list of products and respective *m/z* assignments.

TABLE 3

Observed and theoretical *m/z* for all products in primer-template complex shown in Fig. 3

Product	*m/z* observed	*m/z* theoretical
5′-pTAATGA-3′	Not observed	(−1) 1894.24, (−2) 946.62
5′-pTCATGA-3′	(−2) 934.64	(−1) 1870.22, (−2) 934.60
5′-pTCATGAG-3′	(−2) 1099.27, (−3) 732.27	(−2) 1099.21, (−3) 732.47
5′-pTCATGAA-3′	(−2) 1091.27, (−3) 727.00	(−2) 1091.21, (−3) 727.14

TABLE 4

Observed and theoretical *m/z* for all products in primer-template complex shown in Fig. 4

Product	*m/z* observed	*m/z* theoretical
5′-pCATGCA-3′	(−2) 926.64	(−1) 1855.20, (−2) 927.10
5′-pCATGCAG-3′	(−2) 1091.64, (−3) 727.55	(−2) 1091.70, (−3) 727.47
5′-pCATGCAA-3′	(−2) 1083.09, (−3) 722.09	(−2) 1083.70, (−3) 722.13
5′-pCCTGCA-3′	(−2) 915.00	(−1) 1831.18, (−2) 915.08
5′-pCCTGCAG-3′	(−2) 1079.64, (−3) 719.27	(−2) 1079.69, (−3) 719.46
5′-pCCTGCAA-3′	(−2) 1071.64, (−3) 713.91	(−2) 1071.69, (−3) 714.12

(8-oxoG)AT GAC GCT)-3′ paired to primer 5′-d(AGC GTC AT)-3′ and dCMPNPP, dAMPNPP, or dGMPNPP opposite 8-oxoG (Ci, Ai, and Gi complexes, respectively; i indicates insertion). For a full list of oligonucleotide constructs used, please see Table 6. To prevent the primer from being extended during crystallization in the presence of Mg^{2+}, we used dNMPNPP analogs instead of dNTPs. The crystal structure of the complex with the same template-primer duplex and incoming dCMPNPP opposite native G served as the reference (Cn complex; n indicates native). The crystal structures of the Cn, Ci, Ai, and Gi complexes were all determined at resolutions of between 1.5 and 1.8 Å (Table 7). In the structures, all residues of the catalytic core of hpol η were visible in the electron density with very few exceptions (Table 7). The 5′-terminal C and A nucleotides in the template strand are disordered in the structures, and the T adjacent to the lesion exhibits high conformational flexibility. Examples of the quality of the final electron density and views of the active sites are depicted in Fig. 5.

The structure of the G:dCMPNPP pair at the active site of the Cn complex reveals the expected Watson-Crick geometry (Fig. 6*A*). A very similar configuration of the active site is seen in the Ci complex with template 8-oxoG opposite incoming dCMPNPP, with the nucleoside lesion in the *anti* conformation and thus establishing three H-bonds with cytosine (Fig. 6*B*). In both cases, amino acids from the hpol η finger domain engage in contacts to the nascent base pair. On the template side, Gln-38 Nε donates in an H-bond to N3 of 8-oxoG (or G in the native template) from the minor groove side. On the primer side, the side chain of Arg-61 adopts a coiled conformation and stacks on top of the base of the incoming nucleotide (Fig. 6*B*, *right*). In addition to the stacking interaction, Arg Nη forms an H-bond to the β-phosphate group of dCMPNPP. The distances

TABLE 5
LC-MS/MS analysis of full-length extension products

Primer/template	% of total	% C	% A	Ref.
Product 5′-TAATGA-3′	0	100	<1	This work
Product 5′-TCATGA-3′	15			
Product 5′-TCATGAG-3′	21			
Product 5′-TCATGAA-3′	64			
Template 3′-A***X***TACT-5′				
Product 5′-CATGCA-3′	2	80	20	45
Product 5′-CATGCAG-3′	8			
Product 5′-CATGCAA-3′	10			
Product 5′-CCTGCA-3′	1			
Product 5′-CCTGCAG-3′	29			
Product 5′-CCTGCAA-3′	50			
Template 3′-G*X*ACGT-5′				
Product 5′-CAGGCG-3′	4	90	10	46
Product 5′-CAGGCGG-3′	1			
Product 5′-CAGGCGA-3′	5			
Product 5′-CCGGCG-3′	46			
Product 5′-CCGGCGG-3′	9			
Product 5′-CCGGCGA-3′	28			
Product 5′-CCGGCGC-3′	7			
Template 3′-G*X*CCGC-5′				
Product 5′-TAGGAA-3′	0	97	3	47
Product 5′-TAGGAAA-3′	3			
Product 5′-TCGGAA-3′	25			
Product 5′-TCGGAAG-3′	18			
Product 5′-TCGGAAA-3′	46			
Product 5′-TCGGAAC-3′	8			
Template 3′-A*X*CCTT-5′				
Product 5′-AACGTC-3′	1	83	17	42
Product 5′-AACGTCG-3′	7			
Product 5′-AACGTCA-3′	9			
Product 5′-ACCGTC-3′	1			
Product 5′-ACCGTCG-3′	20			
Product 5′-ACCGTCA-3′	58			
Product 5′-ACCGTCC-3′	4			
Template 3′-T*X*GCAG-5′				
Product 5′-CACAGT-′	0	100	<1	35
Product 5′-CCCAGT-3′	3			
Product 5′-CCCAGTG-3′	40			
Product 5′-CCCAGTA-3′	53			
Product 5′-CCCAGTC-3′	4			
Template 3′-G*X*GTCA-5′				

TABLE 6
DNA sequences used in crystallization of hpol η-DNA complexes

Structure name	DNA sequence	Incoming nucleotide
G:dCTP reference (Cn)	3′-TCG CAG TAG TAC-5′ 5′-AGC GTC AT-3′	dCMPNPP
8-OxoG:dCTP (Ci)	3′-TCG CAG TA(8OG) TAC-5′ 5′-AGC GTC AT-3′	dCMPNPP
8-OxoG:dATP (Ai)	3′-TCG CAG TA(8OG) TAC-5′ 5′-AGC GTC AT-3′	dAMPNPP
8-OxoG:dGTP (Gi)	3′-TCG CAG TA(8OG) TAC-5′ 5′-AGC GTC AT-3′	dGMPNPP
8-OxoG:C extension (Ce)	3′-TCG CAG T(8OG)G TAC-5′ 5′-AGC GTC AC-3′	dCMPNPP
8-OxoG:A extension (Ae)	3′-TCG CAG T(8OG)G TAC-5′ 5′-AGC GTC AA-3′	dCMPNPP

between O3′ from the 3′-terminal T of the primer and Pα of the incoming nucleotide triphosphate in the Cn and Ci complexes are 3.27 and 3.24 Å, respectively. The angle (pT)O3′···Pα–N(Pβ) between nucleophile and scissile bond in the Cn complex was 177.9°, and in the Ci complex the corresponding angle was 176.8°.

Opposite both incoming dAMPNPP in the Ai complex and dGMPNPP in the Gi complex, 8-oxoG is in the *syn* conformation and thus presents its Hoogsteen edge to the nucleotide triphosphates. Gln-38 Nε now donates in an H-bond to O8 of 8-oxoG that is pointing into the minor groove. The 8-oxoG:dAMPNPP pair is stabilized by H-bonds between $N6(H)_2$ (A) and O6 (8-oxoG) and between N1 (A) and N7(H) (8-oxoG) (Fig. 6*C*). Arg-61 has shifted its position relative to the active sites in the Cn and Ci complexes, and there is no overlap between its side chain and adenine consistent with stacking (Fig. 6*C*, *right*). However, Arg Nη still forms an H-bond with the β-phosphate of dAMPNPP. Compared with the Ci complex, the distance between O3′ from the 3-terminal T of the primer and Pα of dAMPNPP is slightly shorter (3.13 Å). The (pT)O3′···Pα–N(Pβ) angle was 176.0°.

In the active site harboring 8-oxoG:dGMPNPP, the side chain of Arg-61 no longer adopts the coiled conformation seen in the structures with dAMPNPP and dCMPNPP opposite the adduct. Instead, the side chain adopts a more or less extended conformation, thus allowing the Nη groups of the guanidino moiety to establish H-bonds to O6 of both 8-oxoG and dGMPNPP in the major groove (Fig. 6*D*). The latter interaction is possible because the base of the incoming nucleotide has been pushed into the minor groove relative to both the structures with incoming dCMPNPP or with incoming dAMPNPP (Fig. 7). As a result, one of the two H-bonds established between 8-oxoG and dGMPNPP involves the 8-oxygen of the former (Fig. 4*D*), whereas this oxygen is not involved in an H-bond in the 8-oxoG:dAMPNPP pair (Fig. 6*C*). Along with this movement of the incoming nucleotide, the 3′-terminal T of the primer has also changed its orientation relative to the structures of the Cn, Ci, and Ai complexes (Figs. 6*D*, and 7). The distance between O3′ (T) and Pα is considerably longer (3.71 Å), and the 3′-hydroxyl group is no longer positioned more or less in line with the scissile P–O bond as in the other complexes, but rather it assumes an adjacent orientation (angle 89.5°; Fig. 6*D*).

X-ray Crystallography of Ternary hpol η-DNA-dNTP Extension-step Complexes—To visualize the active site geometries and relative orientations of incoming nucleotide triphosphate and DNA primer at the extension stage, following insertion of either dCTP or dATP opposite 8-oxoG, we determined two additional hpol η crystal structures. The structures of the ternary complexes between the polymerase, the template-primer duplex 5′-d(CAT G(8-oxoG)T GAC GCT)-3′:5′-d(AGC GTC A*X*)-3′ (*X* = dC or dA), and dCMPNPP were determined at 1.72 and 1.62 Å resolution, respectively. Selected crystal data and refinement parameters for these Ce (extension of 8-oxoG:C pair) and Ae (extension of 8-oxoG:A) complex structures are given in Table 7. Illustrations of the active site configurations in the complexes and the quality of the final electron density are depicted in Fig. 5, *E* (Ce complex) and *F* (Ae complex). In the Ce complex, the nascent dG:dCMPNPP pair stacks on top of *anti* 8-oxoG:dC, and in the Ae complex the same nascent pair stacks on top of *syn* 8-oxoG:dA. The orientation of Arg-61 from the finger domain relative to the base plane of the incoming nucleotide is very similar to that observed in the structure of the Cn and Ci complexes. Thus, the curled conformation of the arginine side chain results in extensive overlap with the cytosine. On the side of the template strand, Gln-38 contacts the N3 atom of G in the minor groove, but it is too short to reach down to 8-oxoG at the −1 position either in the *anti* conformation opposite dC or in the *syn* conformation opposite dA (Fig. 8). The superimposition of the two complexes reveals closely sim-

TABLE 7
Crystal data, data collection parameters and structure refinement statistics

Complex	G:dCMPNPP (Cn)	8-OxoG:dCMPNP (Ci)	8-OxoG:dAMPNPP (Ai)	8-OxoG:dGMPNPP (Gi)	8-OxoG:C (Ce)	8-OxoG:A (Ae)
Data collection						
Wavelength Å	1.07810 Å	0.97872 Å	1.07810 Å	0.97872 Å	0.97872 Å	0.97872 Å
Space group	$P6_1$	$P6_1$	$P6_1$	$P6_1$	$P6_1$	$P6_1$
Resolution	42.24 to 1.58 Å (1.64 to 1.58 Å)[a]	42.52 to 1.72 Å (1.78 to 1.72 Å)	42.68 to 1.70 Å (1.76 to 1.70 Å)	42.59 to 1.72 Å (1.78 to 1.72 Å)	42.57 to 1.72 Å (1.78 to 1.72 Å)	42.70 to 1.62 Å (1.68 to 1.62 Å)
Unit cell $a = b$, c	98.66, 81.79 Å	98.20, 81.55 Å	98.57, 81.56 Å	98.37, 81.70 Å	98.31, 81.60 Å	98.61, 81.84 Å
Unique reflections	61,923 (6,148)	47,424 (4,714)	49,367 (4,854)	47,675 (4,752)	47,720 (4,725)	57,391 (5,696)
Completeness [%]	99.9 (99.7)	99.9 (99.7)	99.5 (98.6)	99.9 (99.9)	99.7 (99.0)	100.0 (100.0)
I/σ(I)	20.86 (2.33)	23.73 (4.29)	15.65 (1.92)	18.35 (2.93)	26.32 (3.94)	15.33 (3.21)
Wilson B-factor	19.4 $Å^2$	19.1 $Å^2$	23.7 $Å^2$	21.0 $Å^2$	21.1 $Å^2$	17.1 $Å^2$
R-merge	0.065 (0.863)	0.070 (0.647)	0.064 (0.948)	0.082 (0.827)	0.065 (0.755)	0.099 (0.806)
Redundancy	7.4 (7.2)	7.3 (6.7)	7.4 (6.9)	7.5 (7.4)	7.2 (6.6)	7.4 (6.5)
Refinement						
R-work	0.170 (0.233)	0.163 (0.211)	0.172 (0.244)	0.185 (0.271)	0.172 (0.228)	0.162 (0.199)
R-free	0.215 (0.269)	0.208 (0.253)	0.219 (0.294)	0.232 (0.351)	0.210 (0.270)	0.204 (0.238)
No. of atoms protein/DNA	3,459/409	3,470/410	3,441/410	3,517/430	3,380/409	3,445/413
dNMPNPP/Mg^{2+}	28/2	28/2	30/2	31/2	28/2	28/2
Water/solute	475/6	466/12	424/6	462/6	452/6	532/12
Protein residues	450	451	451	450	447	449
Average B-factor	26.0	24.4	30.7	26.6	28.6	24.4
Protein/DNA	24.9/27.3	23.1/26.8	29.7/31.5	25.2/31.3	27.4/31.4	23.1/26.4
dNMPNPP/Mg^{2+}	15.2/13.6	12.1/10.6	18.8/13.5	16.7/14.8	16.4/17.8	13.0/19.6
Water/solute	33.0/16.7	32.7/21.7	38.0/23.1	34.3/18.1	36.2/17.9	31.7/22.4
r.m.s.[b] (bonds)	0.019	0.015	0.017	0.014	0.012	0.015
r.m.s. (angles)	1.8	1.4	1.5	1.2	1.2	1.4
Ramachandran, favored	98%	98%	97%	97%	98%	98%
Ramachandran, outliers	0.23%	0.23%	0.46%	0.22%	0.47%	0.46%

[a] Statistics for the highest resolution shell are shown in parentheses.
[b] r.m.s. is root mean square.

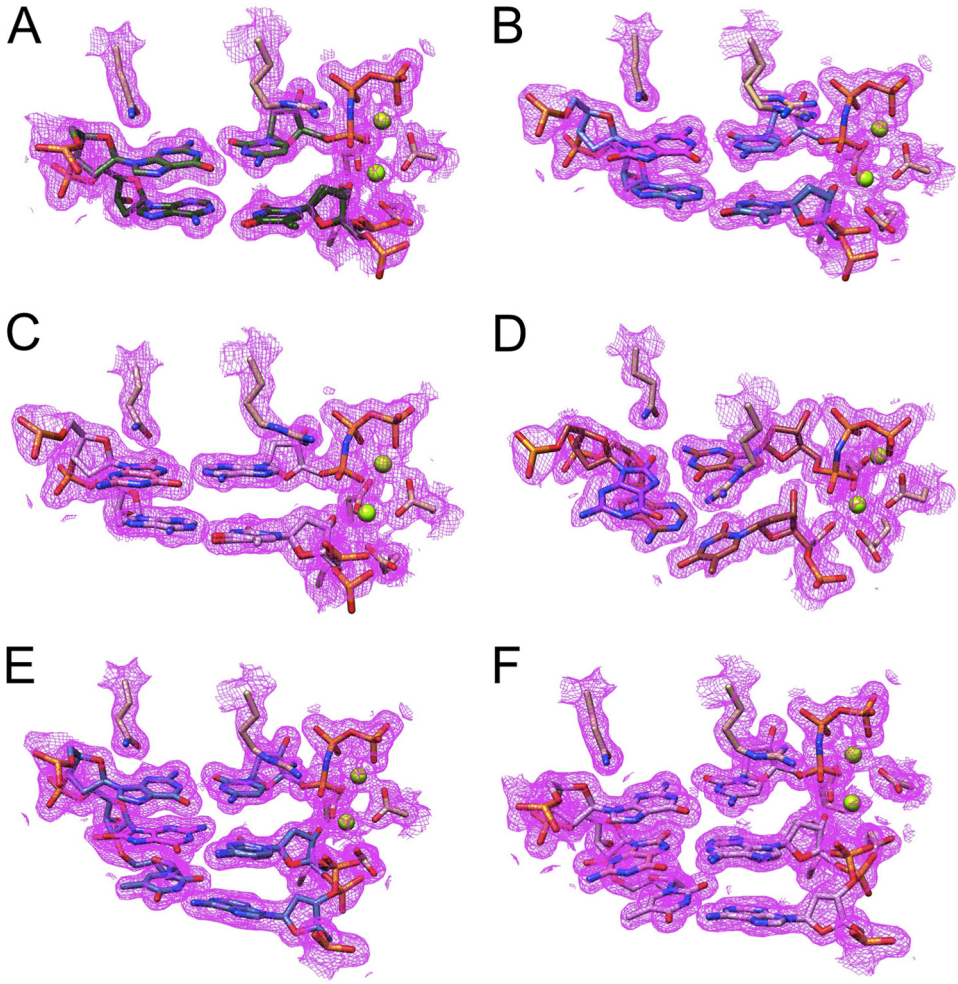

FIGURE 5. **Quality of the final electron density in the insertion- and extension-step complexes between hpol η and 8-oxoG-adducted template-primer duplexes.** The Fourier ($2F_o - F_c$) sum electron density around 8-oxoG and neighboring base pairs in the Cn (*A*), Ci (*B*), Ai (*C*), Gi (*D*), Ce (*E*), and Ae (*F*) complexes (see Table 6 for DNA sequences) is drawn at the 1σ threshold. The two depicted polymerase side chains are from Gln-38 (*top left* in panels) and Arg-61 (*top right* in panels), and Mg^{2+} ions are *light green spheres*.

ilar active site geometries relative to orientations between the 3-terminal residue of the primer and the incoming dCMPNPP and positions of Mg^{2+} ions (Fig. 6*C*). The distance between O3′ (T) and Pα in the Ce complex amounts to 3.38 Å, and the corresponding distance in the Ae complex is 3.35 Å. Together, these structures demonstrate convincingly that, unlike during the insertion steps, once hpol η has incorporated either dC or dA opposite the 8-oxoG adduct, the different pairing modes of the resulting 8-oxoG:C and 8-oxoG:A pairs are of little consequence for the relative orientations of primer strand and the next incoming nucleotide.

DISCUSSION

Although 8-oxoG is the most common oxidative damage product in DNA and pol η is considered important for TLS past the adduct, the human enzyme has hitherto not been subjected to a detailed kinetic (*i.e.* pre-steady-state level) and three-dimensional structural investigation in the context of 8-oxoG bypass. Our analysis addresses this void and provides a complete kinetic and structural framework for hpol η bypass of this major oxidative damage product. The steady-state results indicate a somewhat lower efficiency (k_{cat}/K_m) of dCTP incorporation opposite 8-oxoG relative to the corresponding process opposite G (~30%). The efficiency of dATP incorporation opposite 8-oxoG is increased 136-fold relative to dATP:G, a difference that translates into a 280-fold change in the frequency of insertion in favor of dATP:8-oxoG. A further finding of the steady-state kinetic study is that hpol η has an increased tendency to insert dGTP opposite 8-oxoG relative to template G (8-fold at the level of efficiency k_{cat}/K_m), although both processes are negligible compared with both dCTP and dATP insertion (the frequency of dGTP:8-oxoG insertion is reduced 10-fold compared with dATP:8-oxoG). The steady-state results support the notion that hpol η bypasses 8-oxoG efficiently and with limited error. The pre-steady-state results confirm this conclusion in that the insertions of dCTP opposite both G and 8-oxoG exhibit burst phases with the burst amplitude and burst rate (k_p) being in favor of insertion opposite G. By comparison, the insertion of dATP opposite 8-oxoG did not display a true burst, and the apparent rate was reduced (Fig. 2*D*). These data are consistent with a clear kinetic advantage of dCTP incorporation opposite 8-oxoG over dATP by hpol η.

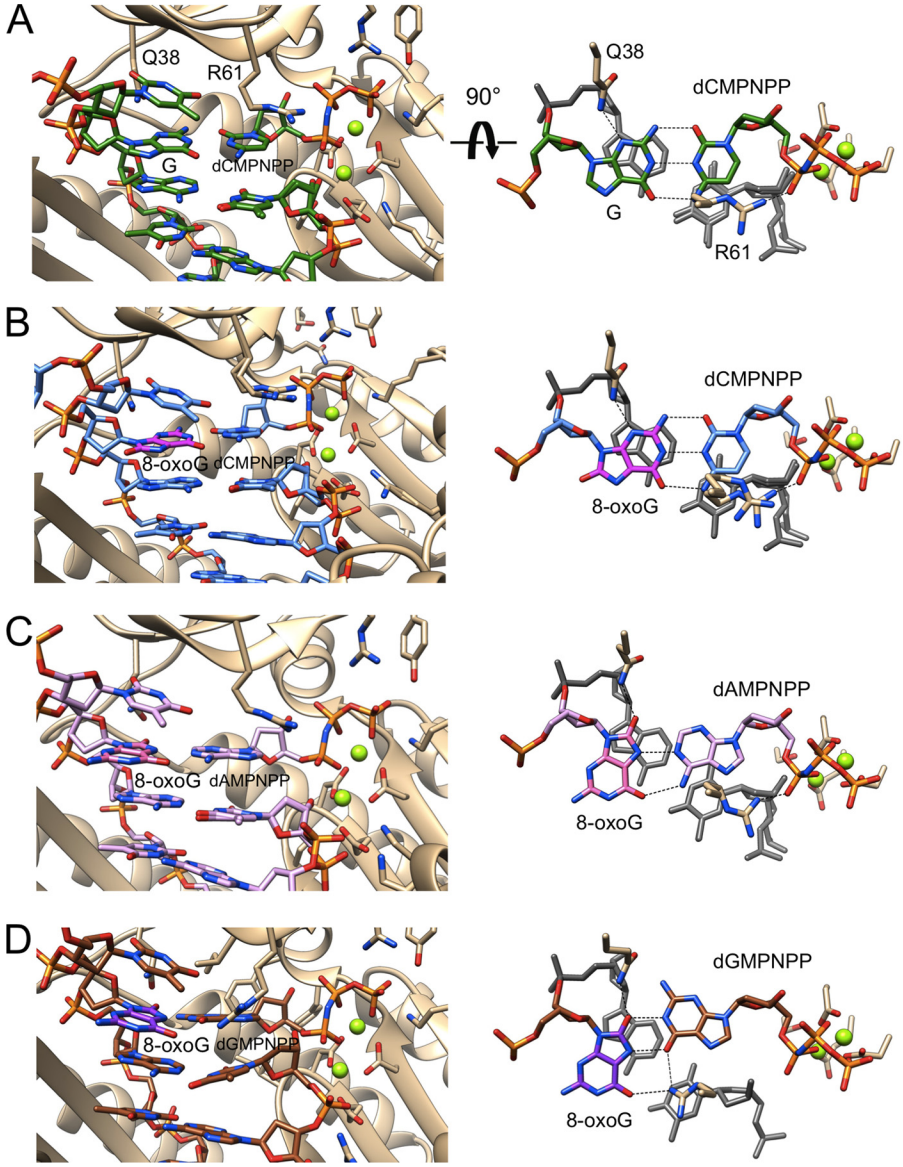

FIGURE 6. **Active site conformations and base pairing configurations in hpol η-DNA-dNMPNPP insertion-step complexes.** Views are into the active sites from the major groove side (panels on the *left*) and rotated by 90° around the horizontal axis and looking roughly along the normal to the nucleobase plane of the incoming dNMPNPP (panels on the *right*) for four hpol η complexes. The polymerase is shown as a schematic, and the DNA template-primer duplex and selected hpol η side chains are shown in *stick* form (*e.g.* finger residues Gln-38 and Arg-61; carbon atoms colored in *beige*). Oxygen, nitrogen, and DNA phosphorus atoms are colored in *red, blue,* and *orange*, respectively, and Mg^{2+} ions are drawn as *light green spheres*. Hydrogen bonds are *dashed lines*. *A*, complex with template G paired to incoming dCMPNPP (reference structure). DNA carbon atoms are *green*. *B*, complex with template 8-oxoG paired to dCMPNPP. DNA carbon atoms are *light blue* except for 8-oxoG carbons that are highlighted in *magenta*. Arg-61 and the primer 3′-terminal T adopt two alternative conformations. *C*, complex with template 8-oxoG paired to dAMPNPP. DNA carbon atoms are *lilac* except for 8-oxoG carbons that are highlighted in *pink*. *D*, complex with template 8-oxoG paired to dGMPNPP. DNA carbon atoms are *brown* except for 8-oxoG carbons that are highlighted in *purple*.

The results of the kinetic analysis here can be compared with those obtained previously from the kinetics of 8-oxoG bypass catalyzed by the pol Dpo4 from *S. solfataricus* (30). Dpo4 was found to exhibit a favorable efficiency of dCTP incorporation opposite 8-oxoG relative to dATP:8-oxoG, and the k_p value of dCTP incorporation opposite 8-oxoG at the pre-steady-state level was nearly double that of the k_p value for dCTP incorporation opposite G (2.3 s^{-1} *versus* 1.3 s^{-1}, respectively; both were considerably lower than the values reported here for hpol η). As well, the activation energy for dCTP incorporation opposite the adduct by Dpo4 was considerably lower than that for incorporation of dCTP opposite the native template G (30). These observations support the general view that Dpo4 displays a behavior that is more similar to that of hpol η but is clearly distinct from its genetic homolog, hpol κ. We reported earlier that hpol κ bypasses 8-oxoG in an error-prone fashion (32). For example, the k_p values of insertions of dATP and dCTP opposite the adduct were 8.2 and 0.4 s^{-1}, respectively, and only the former process was consistent with a burst phase. The LC-MS/MS-based analyses of the full-length extension products of *in vitro* primer bypass past 8-oxoG carried out for all three polymerases (Table 5) (this work and Refs. 30, 32) are also supportive of the similar behaviors of hpol η and Dpo4, *i.e.* nearly error-free bypass of 8-oxoG and relatively error-prone bypass by hpol

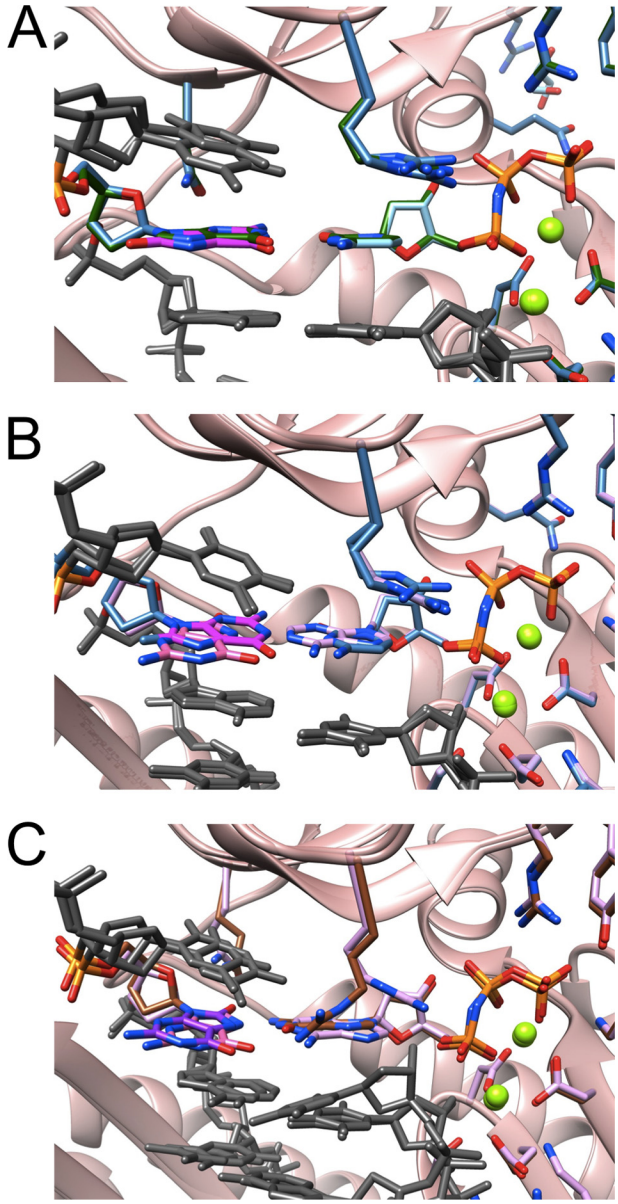

FIGURE 7. **Superimpositions of individual hpol η-DNA-dNMPNPP insertion-step complexes.** All views are into the major groove, and color codes match those used in Fig. 6 except that the protein is colored in *pink*, and the coloring of protein side chains in the individual structures matches that of the incoming dNMPNPP. The template thymidine residue 5′-adjacent to 8-oxoG and the −1 and −2 base pairs are shown in *gray*. *A*, superimposition of the complexes with G:dCMPNPP (*green carbons*) and 8-oxoG:dCMPNPP (*light blue carbons*; 8-oxoG carbons are highlighted in *magenta*). *B*, superimposition of the complexes with 8-oxoG:dCMPNPP (*light blue carbons*; 8-oxoG carbons highlighted in *magenta*) and 8-oxoG:dAMPNPP (*lilac carbons*; 8-oxoG carbons are highlighted in *pink*). *C*, superimposition of the complexes with 8-oxoG:dAMPNPP (*lilac carbons*; 8-oxoG carbons highlighted in *pink*) and 8-oxoG:dGMPNPP (*brown carbons*; 8-oxoG carbons are highlighted in *purple*).

κ. Dpo4 preferred dCTP over dATP with a ratio of 19:1 (30), and hpol κ preferred dATP over dCTP with a ratio of 4:1 (32). In the work presented here, we found that hpol η has an even higher preference for dCTP than Dpo4, *i.e.* the analysis of full-length extension products by LC-MS/MS is consistent with <1–3% incorporation of dATP opposite 8-oxoG in three of the six sequences examined and 10–20% in the other three.

The mass spectrometric analysis of the extension products (not only of the sequence used for the kinetic and structural studies here but also five further sequences previously investigated by others and featuring different nearest neighbors of 8-oxoG) largely attests to the ability of hpol η to bypass 8-oxoG in a largely error-free fashion (Table 5). Accuracies of bypass varied between basically error-free in this study and two previous investigations relying on different sequences (35, 47) and about 4:1 in favor of dCTP (42, 45). In the case of the sequence employed in this study for kinetics and x-ray crystallography (first one shown under "Experimental Procedures" and in Table 5), the LC-MS/MS analysis of full-length extension products demonstrated convincingly that hpol η discriminates against dATP opposite 8-oxoG at both the insertion and extension steps. Thus, no single oligonucleotide product contained a major fraction of A as a consequence of insertion opposite the adduct, supporting the idea that discrimination occurs during both insertion and extension and is consistent with higher fidelity in LC-MS/MS relative to single nucleoside triphosphate insertion assays (Figs. 1 and 2 and Tables 1 and 2). The main insights gained from the kinetic and LC-MS/MS results are that dCTP is overwhelmingly preferred over dATP by hpol η opposite 8-oxoG and that this bias is kinetically controlled, potentially as a result of an active site configuration that guarantees preferred accommodation of the incoming dCTP.

Although our steady-state kinetic analysis cannot shed light on the relative accuracies of the insertion and extension steps as it was done with individual dNTPs and thus provides information only on the insertion of each (opposite 8-oxoG), the mass spectrometric analysis does. The LC-MS analysis is of the fully extended products, which is a measure of misincorporation opposite the adduct (8-oxoG) and the proclivity to extend various pairs (*e.g.* 8-oxoG:C, 8-oxoG:A, and 8-oxoG:G). Thus, a polymerase could efficiently insert a base opposite 8-oxoG but be incapable of extension, leading to differences. Apparently that happens with 8-oxoG:A pairing.

In addition to a reference structure (template G:dCMPNPP; Cn), we determined three crystal structures of hpol η with dCMPNPP (Ci), dAMPNPP (Ai), or dGMPNPP (Gi) opposite template 8-oxoG. Moreover, the structures of complexes with either 8-oxoG:C (Ce) or 8-oxoG:A (Ae) at the −1 position were determined at a similar resolution. The two latter complexes display nearly identical active site configurations (Fig. 8*C*), thereby corroborating the earlier observations and conclusions from kinetics and the LC-MS/MS analysis. Thus, the structural data indicate that the polymerase may extend equally well from either 8-oxoG:C or 8-oxoG:A. Therefore, the absence of A revealed by the mass spectrometric dissection of the full-length extension products needs to be attributed to a less favorable interaction with dATP relative to dCTP during the insertion step of 8-oxoG TLS. The insertion-step structures show that the nascent base pair is probed by two amino acids from the finger domain, Gln-38 and Arg-61 (Fig. 6). Both were identified as conserved residues unique to pol η (28) and were found to play important roles in the bypass by the polymerase of cyclic pyrimidine dimer (52) and cisplatinated DNA (55). However, as far as bypass of 8-oxoG by hpol η is concerned, Gln-38 is not likely to influence accuracy in a decisive manner. This is because the finger residue can interact either with N3 of 8-oxoG in the *anti* conformation and thus be ready to receive

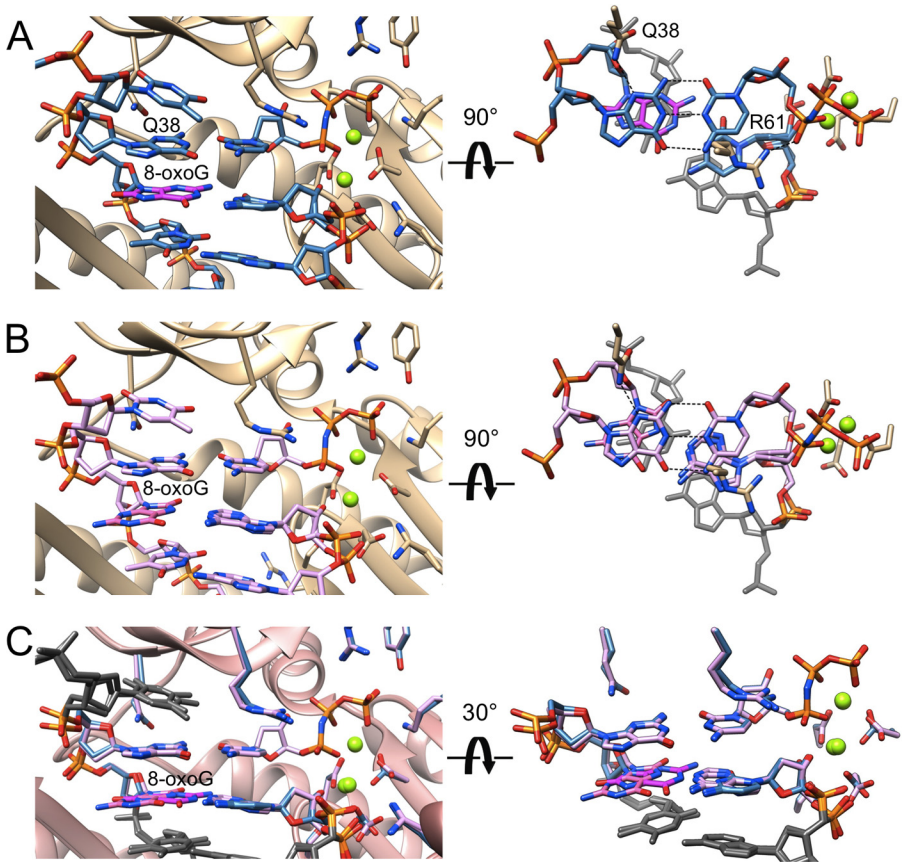

FIGURE 8. **Active site conformations and base pairing configurations in hpol η-DNA-dCMPNPP extension-step complexes.** Views into the active sites from the major groove side (panels on the *left*) and rotated by 90° around the horizontal axis and looking roughly along the normal to the nucleobase plane of the incoming dCMPNPP (*right-hand side panels* in *A* and *B*) and 30° rotation around the horizontal axis in *C* for two hpol η complexes. Drawing mode and color codes match those in Figs. 6 and 7, *i.e.* protein backbone and carbon atoms of selected side chains are colored in *beige* in *A* and *B* and in *pink* (backbone) with side chains matching the coloring of primer C opposite 8-oxoG in the −1 base pair in *C*. The thymidine residue 5′-adjacent to template dG at the active site and the −2 base pairs are shown in *gray* on the *right* and in *C*. Hydrogen bonds are *dashed lines*. *A*, view of the active site with 8-oxoG:dC at the −1 position and template G opposite incoming dCMPNPP. Carbon atoms are *light blue* except for 8-oxoG carbons that are highlighted in *magenta*. *B*, view of the active site with 8-oxoG:dA at the −1 position and template G opposite incoming dCMPNPP. Carbon atoms are *lilac* except for 8-oxoG carbons that are highlighted in *pink*. *C*, superimposition of the two complexes shown in *A* and *B*.

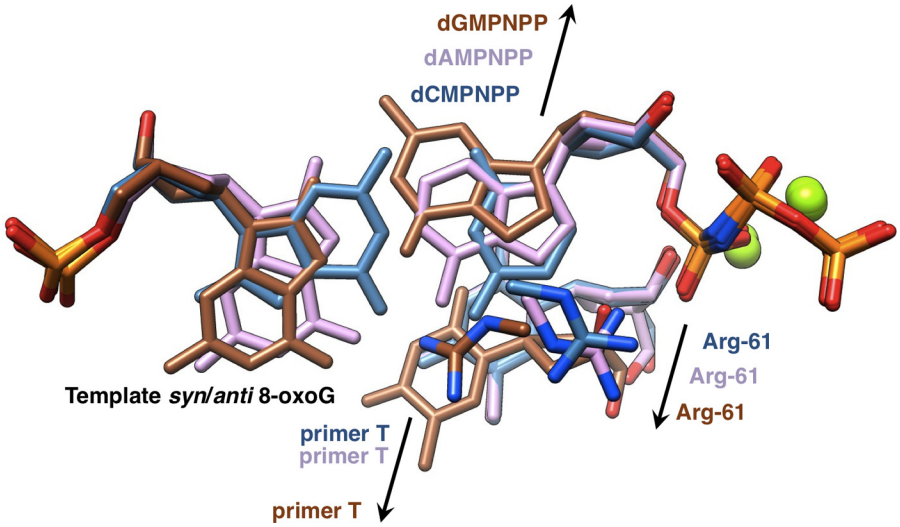

FIGURE 9. **Schematic of the relative orientations of dNMPNPPs and 8-oxoG as well as Arg-61 in the Ci, Ai, and Gi insertion-step hpol η complexes.** *Arrows* indicate the movements of dGMPNPP (*brown*) and dAMPNPP (*lilac*) into the minor groove relative to dCMPNPP (*light blue*), the movements of Arg-61 in the Gi (*brown carbons*) and Ai (*lilac carbons*) complexes into the major groove relative to the Ci complex (*light blue carbons*), and the movement of the 3′-terminal T of the primer in the Gi complex into the major groove relative to the Ai and Ci complexes. The relative movements of the nucleotide triphosphates and Arg-61 in the Gi and Ai complexes result in the loss of stacking between the nucleobase of the incoming dNMPNPP and the guanidino group. The movement of the 3′-terminal T in the Gi complex results in an unfavorable orientation of the 3′-OH for an attack at the α-phosphate group.

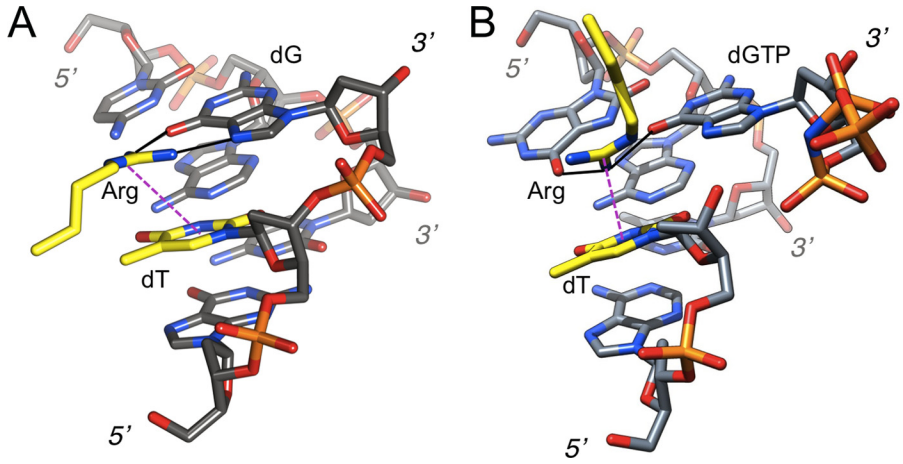

FIGURE 10. **Similar thymine-arginine-guanine interactions in the major grooves of the DNA complexes of yeast sporulation regulator Ndt80 and hpol η.** *A*, sporulation regulator Ndt80 (69) (Protein Data Bank code 1MNN). *B*, human pol η in complex with 8-oxoG adducted template-primer duplex (Gi complex, this work). Carbon atoms of the arginine side chain and the thymine are highlighted in *yellow* and are labeled along with dG (Ndt80) and dGTP (hpol η) and terminal residues; hydrogen bonds are *solid lines* in *black* and the guanidino-thymine cation-π stacking interaction is indicated with a *thin dashed line* in *magenta*. Rather than Arg interacting with the major groove edge of dG that is seen in virtually all structures of DNA-protein complexes, the illustrations convey the particular sequence context and the cation-π stacking interaction in the hpol η complex that are reminiscent of the recognition of 5′-TGTG by tandem arginines by Ndt80 (only one Arg shown in *A*). Differences of course are that in the pol η complex, dG(TP) and T are not covalently bound and that Arg-61 protrudes from the finger domain above, rather than being inserted into the major groove more or less within the guanine plane as in the Ndt80 complex. But just like in the Ndt80-DNA complex, Arg-61 from hpol η pulls out T from the stack, with the consequence that the 3′-hydroxyl group of T is further removed from the α-phosphate of dGTP than in the complexes with dCTP or dATP. In the case of the Ndt80 complex, this particular interaction provides a means of indirect readout; the interaction in the pol η complex is detrimental to activity and explains the low efficiency of dGTP incorporation opposite 8-oxoG (and probably also opposite G).

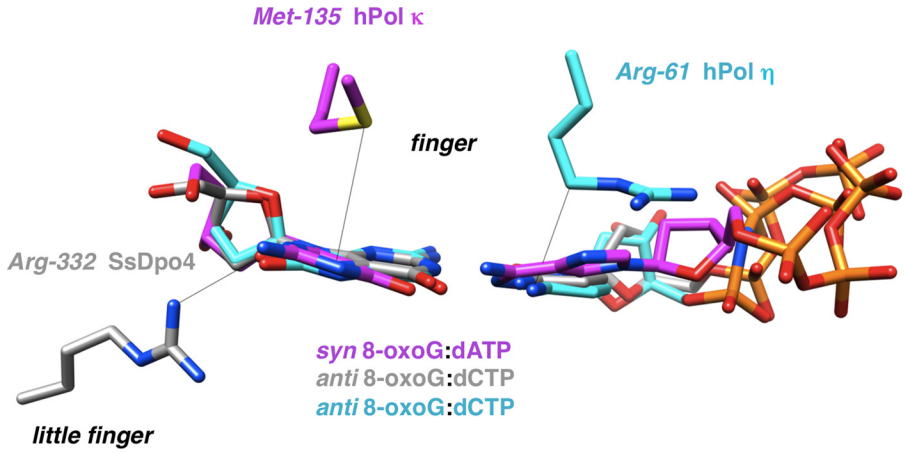

FIGURE 11. **Individual amino acids are key to bypass activity by Y-family DNA polymerases.** Composite of the active sites of *S. solfataricus* Dpo4 (*gray carbons*), hpol κ (*magenta carbons*), and hpol η (*cyan carbons*) with template 8-oxoG opposite incoming dCTP (Dpo4), dCMPNPP (hpol η), or dATP (hpol κ) is shown. Arg-332 in Dpo4 forms an H-bond with O8 of 8-oxoG, and Met-135 in hpol κ and Arg-61 in hpol η engage in stacking interactions with the template adduct and the incoming nucleotide, respectively.

dCTP or O8 of the adducted nucleoside in the *syn* conformation, giving rise to dATP incorporation. Therefore, hpol η does not maintain accuracy of bypass by way of suppressing the tendency of the 8-oxoG nucleoside to adopt the *syn* conformation. Rather it appears to fall to Arg-61 to facilitate accommodation of dCTP in the active site and thus endow it with a kinetic advantage over dATP insertion. Geometric considerations, *i.e.* the position of O3′ from the incoming dNTP relative to the Pα phosphate group, are not suggestive of the preference for dCTP being the result of a faster chemical step compared with dATP. However, comparison between the active sites in the structures of the Ci and Ai complexes brings to light a more optimal interaction between Arg-61 and the cytosine base, involving both the aliphatic portion of the arginine side chain as well as the guanidino moiety (Figs. 7 and 9). Thus, Arg-61 could direct dCTP more optimally into the active site, stabilize its orientation opposite the adduct, and enhance the residence time. Suarez *et al.* (68), using a bacterial forward mutagenesis assay with a 1–511 hpol η R61A construct, found that this mutation has only a limited effect on the bypass efficiency. However, in preliminary site-directed mutagenesis work, we observed that the mutation R61K significantly decreased the fidelity, *i.e.* f(dATP/dCTP catalytic selectivity ratio, Table 1) increased from 0.28 to 0.74. Further studies are planned with more mutants.

Contrary to dCTP and dATP, which exhibit only moderately different orientations relative to the primer and alternative Arg-61 side chain rotamers, dGTP is significantly shifted and therefore in a considerably more unfavorable position for the 3′-OH nucleophile to carry out its attack on the α-phosphate

group (Figs. 7 and 9). The cation-π interaction between Arg-61, now in an extended conformation, and the 3′-T of the primer is reminiscent of the arrangement of arginine pulling T from under the adjacent G in the DNA major groove of the complex with the yeast sporulation regulator Ndt80 (Fig. 10) (69). A similar displacement of the terminal primer base was also seen in the structure of hpol η with a T:dGTP mismatch at the active site (70). These observations underscore the versatile nature of the roles played by the arginine residue in bypass catalysis by hpol η, involving H-bonding, electrostatics, and/or stacking.

Although both hpol η and *S. solfataricus* Dpo4 are capable of bypassing 8-oxoG efficiently and accurately, they rely on entirely different strategies to avoid misincorporation of dATP and subsequent transversion mutation. Unlike pol η, which does not recruit a residue from the LF domain to support accurate 8-oxoG bypass, Dpo4 uses LF residue Arg-332 to prevent 8-oxoG at the 0 (insertion) and −1 (extension) locations from adopting the preferred *syn* conformation by establishing an H-bond between the Arg-332 guanidino moiety and the O8 atom of 8-oxoG (Fig. 11). Therefore, it appears that either interacting with the template strand and the adduct itself or exerting influence on the choice of the incoming nucleotide triphosphate can be successfully used by Y-family pols to catalyze accurate TLS. Both pol η and Dpo4 are likely the polymerases of choice for warding off the negative consequences of oxidative damage in the respective organisms. Conversely, hpol κ bypasses 8-oxoG in an error-prone fashion (32). Like hpol η, hpol κ uses a residue from the finger domain to interact with the nascent base pair (Fig. 11). However, the particular arrangement between Met-135 and template 8-oxoG favors the *syn* conformation of the adducted nucleoside (32, 71). In eukaryotic organisms, the recruitment of pol κ for bypassing the 8-oxoG adduct is deleterious.

Acknowledgments—We are grateful to Dr. L. Lei for help with protein expression and purification, Dr. Z. Wawrzak for assistance with x-ray diffraction data collection at the Advanced Photon Source, Dr. W. Yang for helpful discussions, and K. Trisler for assistance in preparation of the manuscript. Vanderbilt University is a member institution of the Life Sciences Collaborative Access Team at sector 21 of the Advanced Photon Source, Argonne, IL. Use of the Advanced Photon Source at Argonne National Laboratory was supported by the United States Department of Energy, Office of Science, Office of Basic Energy Sciences, under Contract DE-AC02-06CH11357.

REFERENCES

1. Beckman, K. B., and Ames, B. N. (1997) Oxidative decay of DNA. *J. Biol. Chem.* **272,** 19633–19636
2. Helbock, H. J., Beckman, K. B., Shigenaga, M. K., Walter, P. B., Woodall, A. A., Yeo, H. C., and Ames, B. N. (1998) DNA oxidation matters: the HPLC-electrochemical detection assay of 8-oxo-deoxyguanosine and 8-oxo-guanine. *Proc. Natl. Acad. Sci. U.S.A.* **95,** 288–293
3. Kamiya, H. (2004) Mutagenicities of 8-hydroxyguanine and 2-hydroxyadenine produced by reactive oxygen species. *Biol. Pharm. Bull.* **27,** 475–479
4. Degan, P., Shigenaga, M. K., Park, E. M., Alperin, P. E., and Ames, B. N. (1991) Immunoaffinity isolation of urinary 8-hydroxy-2′-deoxyguanosine and 8-hydroxyguanine and quantitation of 8-hydroxy-2-deoxyguanosine in DNA by polyclonal antibodies. *Carcinogenesis* **12,** 865–871
5. Malins, D. C., and Haimanot, R. (1991) Major alterations in the nucleotide structure of DNA in cancer of the female breast. *Cancer Res.* **51,** 5430–5432
6. Fraga, C. G., Shigenaga, M. K., Park, J. W., Degan, P., and Ames, B. N. (1990) Oxidative damage to DNA during aging: 8-hydroxy-2′-deoxyguanosine in rat organ DNA and urine. *Proc. Natl. Acad. Sci. U.S.A.* **87,** 4533–4537
7. Shimoda, R., Nagashima, M., Sakamoto, M., Yamaguchi, N., Hirohashi, S., Yokota, J., and Kasai, H. (1994) Increased formation of oxidative DNA damage, 8-hydroxydeoxyguanosine, in human livers with chronic hepatitis. *Cancer Res.* **54,** 3171–3172
8. Fraga, C. G., Motchnik, P. A., Shigenaga, M. K., Helbock, H. J., Jacob, R. A., and Ames, B. N. (1991) Ascorbic acid protects against endogenous oxidative DNA damage in human sperm. *Proc. Natl. Acad. Sci. U.S.A.* **88,** 11003–11006
9. Beard, W. A., Batra, V. K., and Wilson, S. H. (2010) DNA polymerase structure-based insight on the mutagenic properties of 8-oxoguanine. *Mutat. Res.* **703,** 18–23
10. van Loon, B., Markkanen, E., and Hübscher, U. (2010) Oxygen as a friend and enemy: how to combat the mutational potential of 8-oxo-guanine. *DNA Repair* **9,** 604–616
11. Earley, M. C., and Crouse, G. F. (1998) The role of mismatch repair in the prevention of base pair mutations in *Saccharomyces cerevisiae*. *Proc. Natl. Acad. Sci. U.S.A.* **95,** 15487–15491
12. Nash, H. M., Bruner, S. D., Schärer, O. D., Kawate, T., Addona, T. A., Spooner, E., Lane, W. S., and Verdine, G. L. (1996) Cloning of a yeast 8-oxoguanine DNA glycosylase reveals the existence of a base excision DNA-repair protein superfamily. *Curr. Biol.* **6,** 968–980
13. van der Kemp, P. A., Thomas, D., Barbey, R., de Oliveira, R., and Boiteux, S. (1996) Cloning and expression in *Escherichia coli* of the OGG1 gene of *Saccharomyces cerevisiae*, which codes for a DNA glycosylase that excises 7,8-dihydro-8-oxoguanine and 2,6-diamino-4-hydroxy-5-*N*-methylformamidopyrimidine. *Proc. Natl. Acad. Sci. U.S.A.* **93,** 5197–5202
14. Ni, T. T., Marsischky, G. T., and Kolodner, R. D. (1999) MSH2 and MSH6 are required for removal of adenine misincorporated opposite 8-oxo-guanine in *S. cerevisiae*. *Mol. Cell* **4,** 439–444
15. Friedberg, E. C., Walker, G. C., Siede, W., Wood, R. D., Shultz, R. A., and Ellenberger, T. (eds) (2006) *DNA Repair and Mutagenesis*, 2nd Ed, American Society for Microbiology, Washington, D. C.
16. Bridges, B. A. (2005) Error-prone DNA repair and translesion DNA synthesis II: the inducible SOS hypothesis. *DNA Repair* **4,** 725–726
17. Edmunds, C. E., Simpson, L. J., and Sale, J. E. (2008) PCNA ubiquitination and REV1 define temporally distinct mechanisms for controlling translesion synthesis in the avian cell line DT40. *Mol. Cell* **30,** 519–529
18. Fu, Y., Zhu, Y., Zhang, K., Yeung, M., Durocher, D., and Xiao, W. (2008) Rad6-Rad18 mediates a eukaryotic SOS response by ubiquitinating the 9-1-1 checkpoint clamp. *Cell* **133,** 601–611
19. Lehmann, A. R. (2006) New functions for Y family polymerases. *Mol. Cell* **24,** 493–495
20. Sale, J. E., Lehmann, A. R., and Woodgate, R. (2012) Y-family DNA polymerases and their role in tolerance of cellular DNA damage. *Nat. Rev. Cell Mol. Biol.* **13,** 141–152
21. Prakash, S., Johnson, R. E., and Prakash, L. (2005) Eukaryotic translesion synthesis DNA polymerases: specificity of structure and function. *Annu. Rev. Biochem.* **74,** 317–353
22. Guengerich, F. P. (2006) Interactions of carcinogen-bound DNA with individual DNA polymerases. *Chem. Rev.* **106,** 420–452
23. Eoff, R. L., Egli, M., and Guengerich, F. P. (2010) in *The Chemical Biology of DNA Damage* (Geacintov, N. E., and Broyde, S., eds) pp. 299–330, Wiley-VCH, Weinheim, Germany
24. Yang, W., and Woodgate, R. (2007) What a difference a decade makes: insights into translesion DNA synthesis. *Proc. Natl. Acad. Sci. U.S.A.* **104,** 15591–15598
25. Steitz, T. A. (1999) DNA polymerases: structural diversity and common mechanisms. *J. Biol. Chem.* **274,** 17395–17398
26. Boudsocq, F., Iwai, S., Hanaoka, F., and Woodgate, R. (2001) *Sulfolobus solfataricus* P2 DNA polymerase IV (Dpo4): an archaeal DinB-like DNA polymerase with lesion-bypass properties akin to eukaryotic pol η. *Nucleic Acids Res.* **29,** 4607–4616
27. Ling, H., Boudsocq, F., Woodgate, R., and Yang, W. (2001) Crystal struc-

ture of a Y-family DNA polymerase in action: a mechanism for error-prone and lesion-bypass replication. *Cell* **107,** 91–102
28. Ling, H., Boudsocq, F., Plosky, B. S., Woodgate, R., and Yang, W. (2003) Replication of a *cys-syn* thymine dimer at atomic resolution. *Nature* **424,** 1083–1087
29. Boudsocq, F., Kokoska, R. J., Plosky, B. S., Vaisman, A., Ling, H., Kunkel, T. A., Yang, W., and Woodgate, R. (2004) Investigating the role of the little finger domain of Y-family DNA polymerases in low fidelity synthesis and translesion replication. *J. Biol. Chem.* **279,** 32932–32940
30. Zang, H., Irimia, A., Choi, J.-Y., Angel, K. C., Loukachevitch, L. V., Egli, M., and Guengerich, F. P. (2006) Efficient and high fidelity incorporation of dCTP opposite 7,8-dihydro-8-oxodeoxyguanosine by *Sulfolobus solfataricus* DNA polymerase Dpo4. *J. Biol. Chem.* **281,** 2358–2372
31. Eoff, R. L., Irimia, A., Angel, K. C., Egli, M., and Guengerich, F. P. (2007) Hydrogen bonding of 7,8-dihydro-8-oxodeoxyguanosine with a charged residue in the little finger domain determines miscoding events in *Sulfolobus solfataricus* DNA polymerase Dpo4. *J. Biol. Chem.* **282,** 19831–19843
32. Irimia, A., Eoff, R. L., Guengerich, F. P., and Egli, M. (2009) Structural and functional elucidation of the mechanism promoting error-prone synthesis by human DNA polymerase κ opposite the 7,8-dihydro-8-oxo-2′-deoxyguanosine adduct. *J. Biol. Chem.* **284,** 22467–22480
33. Shibutani, S., Takeshita, M., and Grollman, A. P. (1991) Insertion of specific bases during DNA synthesis past the oxidation-damaged base 8-oxodG. *Nature* **349,** 431–434
34. Hogg, M., Wallace, S. S., and Doublié, S. (2005) Bumps in the road: how replicative DNA polymerases see DNA damage. *Curr. Opin. Struct. Biol.* **15,** 86–93
35. Avkin, S., and Livneh, Z. (2002) Efficiency, specificity and DNA polymerase-dependence of translesion replication across the oxidative DNA lesion 8-oxoguanine in human cells. *Mutat. Res.* **510,** 81–90
36. Lee, D. H., and Pfeifer, G. P. (2008) Translesion synthesis of 7,8-dihydro-8-oxo-2-deoxyguanosine by DNA polymerase η *in vivo*. *Mutat. Res.* **641,** 19–26
37. Rodriguez, G. P., Song, J. B., and Crouse, G. F. (2013) *In vivo* bypass of 8-oxoG. *PLoS Genet.* **9,** e1003682
38. Haracska, L., Yu, S. L., Johnson, R. E., Prakash, L., and Prakash, S. (2000) Efficient and accurate replication in the presence of 7,8-dihydro-8-oxoguanine by DNA polymerase η. *Nat. Genet.* **25,** 458–461
39. Yuan, F., Zhang, Y., Rajpal, D. K., Wu, X., Guo, D., Wang, M., Taylor, J.-S., and Wang, Z. (2000) Specificity of DNA lesion bypass by the yeast polymerase η. *J. Biol. Chem.* **275,** 8233–8239
40. Carlson, K. D., and Washington, M. T. (2005) Mechanism of efficient and accurate nucleotide incorporation opposite 7,8-dihydro-8-oxoguanine by *Saccharomyces cerevisiae* DNA polymerase η. *Mol. Cell Biol.* **25,** 2169–2176
41. Silverstein, T. D., Jain, R., Johnson, R. E., Prakash, L., Prakash, S., and Aggarwal, A. K. (2010) Structural basis for error-free replication of oxidatively damaged DNA by yeast DNA polymerase η. *Structure* **18,** 1463–1470
42. Maga, G., Villani, G., Crespan, E., Wimmer, U., Ferrari, E., Bertocci, B., and Hübscher, U. (2007) 8-Oxo-guanine bypass by human DNA polymerases in the presence of auxiliary proteins. *Nature* **447,** 606–608
43. Markkanen, E., Castrec, B., Villani, G., and Hübscher, U. (2012) A switch between polymerases δ and λ promotes error-free bypass of 8-oxo-G lesions. *Proc. Natl. Acad. Sci. U.S.A.* **109,** 20401–20406
44. Yung, C., Suzuki, T., Okugawa, Y., Kawakami, A., Loakes, D., Negishi, K., and Negishi, T. (2007) Nucleotide incorporation against 7,8-dihydro-8-oxoguanine is influenced by neighboring base sequences in TLS DNA polymerase reaction. *Nucleic Acids Symp. Ser.* **51,** 49–50
45. Zhang, Y., Yuan, F., Wu, X., Wang, M., Rechkoblit, O., Taylor, J.-S., Geacintov, N. E., and Wang, Z. (2000) Error-free and error-prone lesion bypass by human DNA polymerase κ *in vitro*. *Nucleic Acids Res.* **28,** 4138–4146
46. Jaloszyński, P., Masutani, C., Hanaoka, F., Perez, A. B., and Nishimura, S. (2003) 8-Hydroxyguanine in a mutational hotspot of the c-Ha-ras gene causes misreplication, 'action-at-a-distance' mutagenesis and inhibition of replication. *Nucleic Acids Res.* **31,** 6085–6095
47. McCulloch, S. D., Kokoska, R. J., Garg, P., Burgers, P. M., and Kunkel, T. A. (2009) The efficiency and fidelity of 8-oxo-guanine bypass by DNA polymerases δ and η. *Nucleic Acids Res.* **37,** 2830–2840
48. Johnson, R. E., Prakash, S., and Prakash, L. (1999) Efficient bypass of a thymine-thymine dimer by yeast DNA polymerase Polη. *Science* **283,** 1001–1004
49. Masutani, C., Kusumoto, R., Yamada, A., Dohmae, N., Yokoi, M., Yuasa, M., Araki, M., Iwai, S., Takio, K., and Hanaoka, F. (1999) The *XPV* (xeroderma pigmentosum variant) gene encodes human DNA polymerase η. *Nature* **399,** 700–704
50. Johnson, R. E., Kondratick, C. M., Prakash, S., and Prakash, L. (1999) hRAD30 mutations in the variant form of xeroderma pigmentosum. *Science* **285,** 263–265
51. Vaisman, A., Masutani, C., Hanaoka, F., and Chaney, S. G. (2000) Efficient translesion replication past oxaliplatin and cisplatin GpG adducts by human DNA polymerase η. *Biochemistry* **39,** 4575–4580
52. Biertümpfel, C., Zhao, Y., Kondo, Y., Ramón-Maiques, S., Gregory, M., Lee, J. Y., Masutani, C., Lehmann, A. R., Hanaoka, F., and Yang, W. (2010) Structure and mechanism of human DNA polymerase η. *Nature* **465,** 1044–1048
53. Nakamura, T., Zhao, Y., Yamagata, Y., Hua, Y. J., and Yang, W. (2012) Watching DNA polymerase η make a phosphodiester bond. *Nature* **487,** 196–201
54. Alt, A., Lammens, K., Chiocchini, C., Lammens, A., Pieck, J. C., Kuch, D., Hopfner, K. P., and Carell, T. (2007) Bypass of DNA lesions generated during anticancer treatment with cisplatin by DNA polymerase η. *Science* **318,** 967–970
55. Zhao, Y., Biertümpfel, C., Gregory, M. T., Hua, Y. J., Hanaoka, F., and Yang, W. (2012) Structural basis of human polymerase η-mediated chemoresistance to cisplatin. *Proc. Natl. Acad. Sci. U.S.A.* **109,** 7269–7274
56. Lowe, L. G., and Guengerich, F. P. (1996) Steady-state and pre-steady-state kinetic analysis of dNTP insertion opposite 8-oxo-7,8-dihydroguanine by *Escherichia coli* polymerases I exo$^-$ and II exo$^-$. *Biochemistry* **35,** 9840–9849
57. Zang, H., Goodenough, A. K., Choi, J. Y., Irimia, A., Loukachevitch, L. V., Kozekov, I. D., Angel, K. C., Rizzo, C. J., Egli, M., and Guengerich, F. P. (2005) DNA adduct bypass polymerization by *Sulfolobus solfataricus* DNA polymerase Dpo4. Analysis and crystal structures of multiple base-pair substitution and frameshift products with the adduct 1, N^2-ethenoguanine. *J. Biol. Chem.* **280,** 29750–29764
58. Christov, P. P., Angel, K. C., Guengerich, F. P., and Rizzo, C. J. (2009) Replication past the N^5-methyl-formamidopyrimidine lesion of deoxyguanosine by DNA polymerases and an improved procedure for sequence analysis of *in vitro* bypass products by mass spectrometry. *Chem. Res. Toxicol.* **22,** 1086–1095
59. Chowdhury, G., and Guengerich, F. P. (2011) in *Current Protocols Nucleic Acid Chemistry* (Egli, M., Herwijn, P., Matsuda, A., and Sanghvi, Y., eds) pp. 7.16.1–7.16.11, John Wiley and Sons, Inc., Hoboken, NJ
60. Jancarik, J., and Kim, S. H., (1991) Sparse matrix sampling: a screening method for crystallization of proteins. *J. Appl. Crystallogr.* **24,** 409–411
61. Otwinowski, Z., and Minor, W. (1997) Processing of x-ray diffraction data collected in oscillation mode. *Methods Enzymol.* **276,** 307–326
62. Vagin, A., and Teplyakov, A. (2010) Molecular replacement with MOLREP. *Acta Crystallogr. D Biol. Crystallogr.* **66,** 22–25
63. Collaborative Computational Project No. 4 (1994) The CCP4 suite: programs for protein crystallography. *Acta Crystallogr. D Biol. Crystallogr.* **50,** 760–763
64. Adams, P. D., Afonine, P. V., Bunkóczi, G., Chen, V. B., Davis, I. W., Echols, N., Headd, J. J., Hung, L. W., Kapral, G. J., Grosse-Kunstleve, R. W., McCoy, A. J., Moriarty, N. W., Oeffner, R., Read, R. J., Richardson, D. C., Richardson, J. S., Terwilliger, T. C., and Zwart, P. H. (2010) PHENIX: a comprehensive Python-based system for macromolecular structure solution. *Acta Crystallogr. D Biol. Crystallogr.* **66,** 213–221
65. Emsley, P., and Cowtan, K. (2004) Coot: model-building tools for molecular graphics. *Acta Crystallogr. D Biol. Crystallogr.* **60,** 2126–2132
66. Pettersen, E. F., Goddard, T. D., Huang, C. C., Couch, G. S., Greenblatt, D. M., Meng, E. C., and Ferrin, T. E. (2004) UCSF Chimera-a visualization system for exploratory research and analysis. *J. Comput. Chem.* **25,**

1605–1612
67. Choi, J. Y., and Guengerich, F. P. (2005) Adduct size limits efficient and error-free bypass across bulky N2-guanine DNA lesions by human DNA polymerase η. *J. Mol. Biol.* **352,** 72–90
68. Suarez, S. C., Beardslee, R. A., Toffton, S. M., and McCulloch, S. D. (2013) Biochemical analysis of active site mutations of human polymerase η. *Mutat. Res.* **745,** 46–54
69. Lamoureux, J. S., Maynes, J. T., and Glover, J. N. (2004) Recognition of 5′-YpG-3′ sequences by coupled stacking/hydrogen bonding interactions with amino acid residues. *J. Mol. Biol.* **335,** 399–408
70. Zhao, Y., Gregory, M. T., Biertümpfel, C., Hua, Y.-J., Hanaoka, F., and Yang, W. (2013) Mechanism of somatic hypermutation at the WA motif by human DNA polymerase η. *Proc. Natl. Acad. Sci. U.S.A.* **110,** 8146–8151
71. Vasquez-Del Carpio, R., Silverstein, T. D., Lone, S., Swan, M. K., Choudhury, J. R., Johnson, R. E., Prakash, S., Prakash, L., and Aggarwal, A. K. (2009) Structure of human DNA polymerase κ inserting dATP opposite an 8-oxoG DNA lesion. *PLoS ONE* **4,** e5766